Accelerated quantitative multi-material beam hardening correction(BHC) in cone-beam CT

Award:	Certificate of Merit
Poster No.:	C-2161
Congress:	ECR 2012
Type:	Scientific Exhibit
Authors:	Q. Yang, M. Elter, H. Scherl; Erlangen/DE
Keywords:	Artifacts, Computer Applications-3D, Image manipulation / Reconstruction, CT, Research, Radiation physics
DOI:	10.1594/ecr2012/C-2161

Purpose

- In computed tomography (CT), nonlinear characteristics of beam hardening are caused by polychromaticity of x-rays, which severely degrade CT image quality and diagnostic accuracy.
- Current correction approaches used in clinical CT are mainly based on water-equivalent calibration and recent scientific researches published an extension of including dense bones in the scan field. This approach makes assumptions of certain material types, which are only partially valid and may lead to suboptimal corrections. Other correction techniques are limited in correction effectiveness and computational complexity on cone beam geometry, when scanned objects consist of more than one material.
- In this study, we present a new BHC approach which models the polychromatic x-rays with physical characteristics. The aim of our study is to effectively reduce beam hardening with increased applicability to various kinds of datasets for cone beam CT.

Methods and Materials

Methods:

The proposed correction process is illustrated in Fig. 1 on page 5

Original reconstruction:

- The method is initialized by performing a preliminary reconstruction based on FDK[19], from which material distribution can be estimated.

Segmentation:

- Due to the complexity of 3D volume segmentation, a histogram based segmentation algorithm was applied to differentiate materials.
- The main disadvantage of this method is the potential misclassification caused by materials with similar CT numbers and strong streaking artifact.

Ray casting:

- Since the attenuation of a polychromatic x-ray is energy-, distance- and material dependent, the lengths of the ray passing through each material is required for our correction approach. (Fig. 2 on page 5)
- Boundary condition needs to be treated separately to achieve an accurate ray sum at the border of the volume. Binary searching at border voxels of the volume and on material changes are processed. According to computational time and performance, 0.1% of original step size accuracy is used of 10% in processing time increase.

Correction:

1. The total cross sections for each material are calculated from principal photon interactions.
2. To model the polychromatic projections, a logarithm interpolation is used for certain energy levels according to total cross section.
3. Attenuation factors for both monochromatic and polychromatic case are calculated based on total cross section and material density.

Total cross section σ_{total} from the different photon interactions:

$$\sigma_{total} = \sigma_{pe} + \sigma_{coh} + \sigma_{incoh} + \sigma_{pair} + \sigma_{trip} + \sigma_{ph.}$$

Logarithm Interpolation: $\mathcal{L}_E(\sigma) = \frac{\log(E) - \log(E_0)}{\log(E_1) - \log(E_0)} \cdot [\log(\sigma_1) - \log(\sigma_0)]$

At current energy level: $\sigma_{total} = \exp(\mathcal{L}_E(\sigma)) \cdot \sigma_0$

σ_{pe}: atomic photoeffect cross section; σ_{coh}: Rayleigh cross section; σ_{incoh}: incoherent scattering cross secti

Chemical element mass attenuation coefficient $\frac{\mu}{\rho}$:

$$\frac{\mu}{\rho} = \frac{\sigma_{total}}{u \cdot A}$$

μ: attenuation factor; ρ:element density; $u = 1.6605402 \times 10^{-24}$g ; A: relative atomic mass of the target el

Material consisting of compounds:

$$\frac{\mu}{\rho} = \sum_{i=1}^{m} \alpha_i \left(\frac{\mu}{\rho}\right)_i$$

α : fraction by weight of the ith atomic constituent.

Fig. 3: Mathematical derivation for correction steps 1-3.
References: Q. Yang; Erlangen, GERMANY

4. Afterwards, projection intensities are calculated according to intersection lengths between rays and objects.
5. With original projection images as reference, a calibrated correction image can be obtained.

X-ray intensity after passing through single material object:

$$I_{mono} = I_0 e^{-\int \mu ds} \qquad e^{-\int \mu ds} \Rightarrow f($$

$$I_{poly} = \int I_0(E) e^{-\int \mu(s,E) ds} dE \qquad \int e^{-\int \mu(s,E) ds} dE \Rightarrow g$$

X-ray intensity after passing through N-material objects:

$$I_{N,mono} = I_0 \cdot f_1(\mu, d) \cdot f_2(\mu, d) \cdots f_N(\mu, d)$$
$$I_{N,poly} = I_0 \cdot g_1(\mu, d) \cdot g_2(\mu, d) \cdots g_N(\mu, d)$$

Final correction:

$$I_{correction} = \frac{I_{mono}}{I_{poly}} \cdot I_{original}$$

Fig. 4: Mathematical derivation for correction steps 4 and 5.
References: Q. Yang; Erlangen, GERMANY

However, in real x-ray CT applications, some residual artifacts remain that could not be sufficiently suppressed. In particular, dark streaks between dense objects are still present, with an indication of under-correction. Moreover, due to potential inaccuracies of segmentation, overlapping would occur during segmentation and ray casting, which results in both over-correction for low density objects and under-correction for high density objects. Under such circumstances, simple correction factor tuning is no longer effective, and iterative corrections are carried out to improve segmentation accuracy and further mitigate residual artifacts.

Materials:

The validity of the proposed algorithm was evaluated by using real x-ray projected data with several cylindrical objects. Fig. 5 on page 7 shows the chemical composition of these cylinders and reconstructed data without beam hardening correction. The experimental parameters are shown in Table 1 on page 8.

Images for this section:

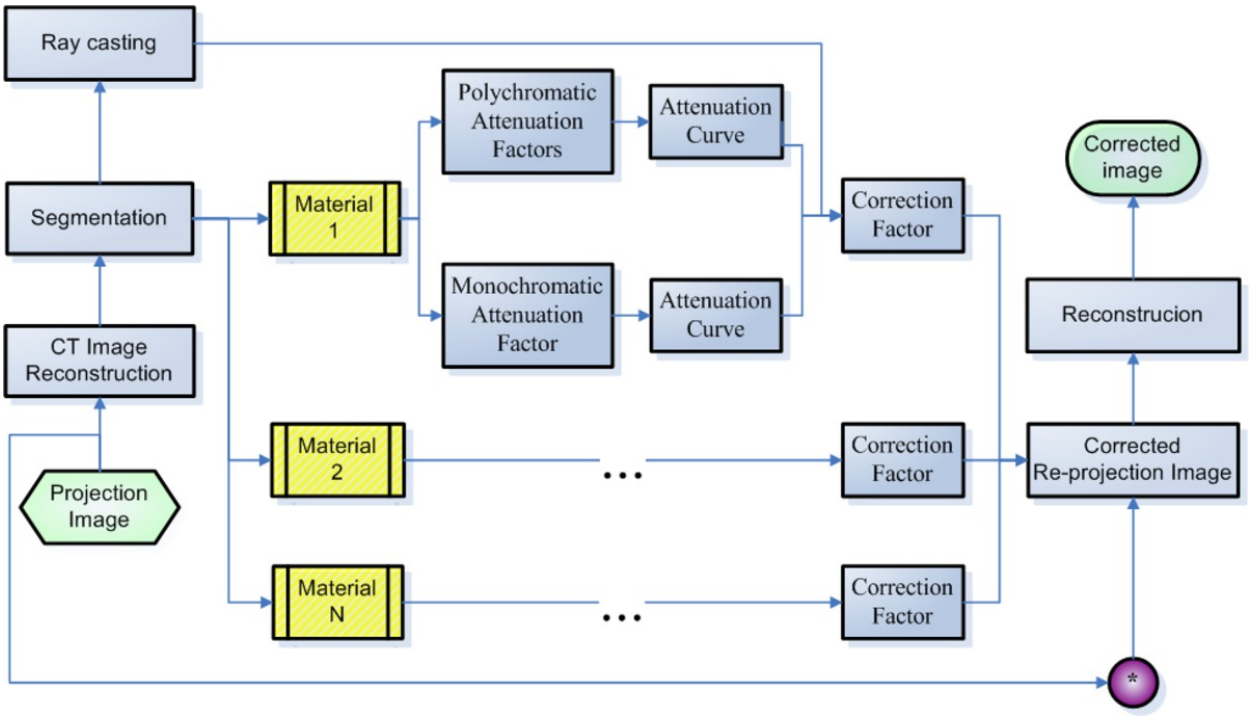

Fig. 1: Flowchart of the proposed beam hardening correction method.

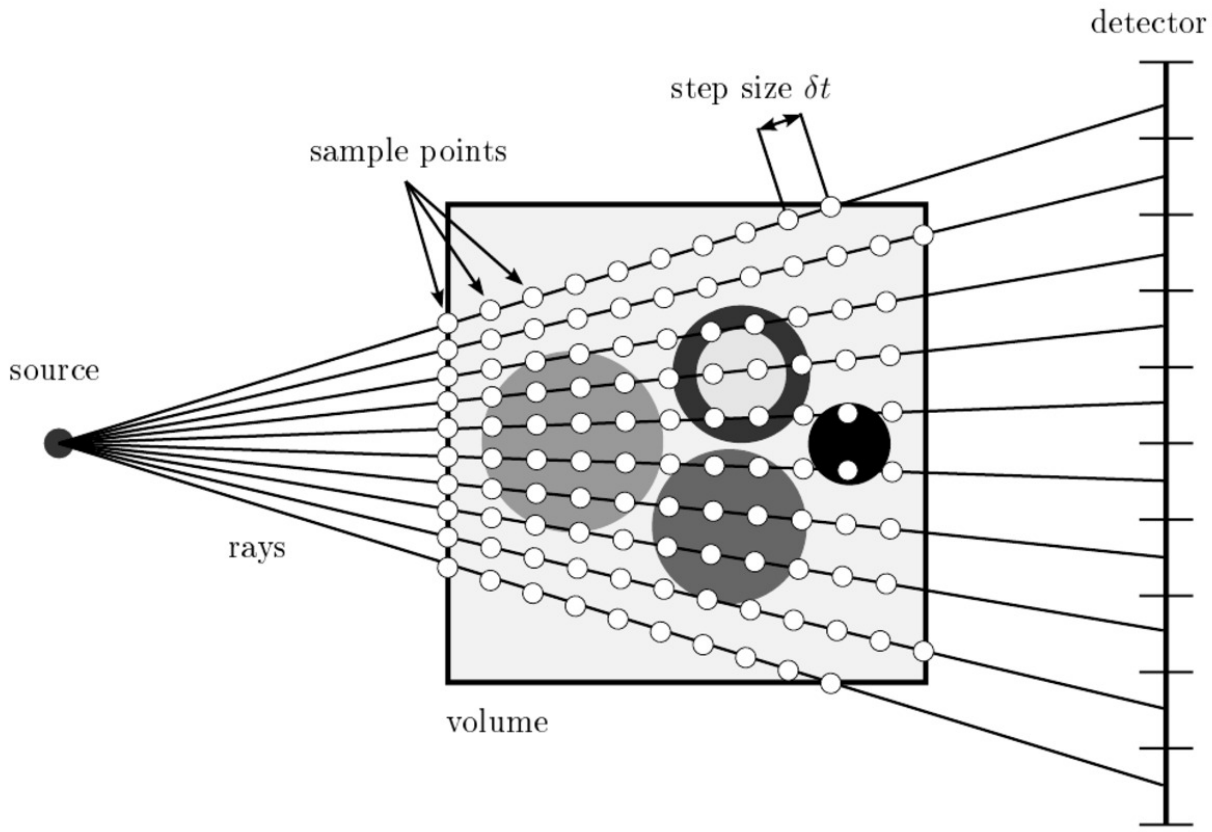

Fig. 2: Illustration of ray casting for calculating intersection lengths between X-rays and objects.

Total cross section σ_{total} from the different photon interactions:

$$\sigma_{total} = \sigma_{pe} + \sigma_{coh} + \sigma_{incoh} + \sigma_{pair} + \sigma_{trip} + \sigma_{ph.n}$$

Logarithm Interpolation: $\mathcal{L}_E(\sigma) = \frac{\log(E) - \log(E_0)}{\log(E_1) - \log(E_0)} \cdot [\log(\sigma_1) - \log(\sigma_0)]$

At current energy level: $\sigma_{total} = \exp(\mathcal{L}_E(\sigma)) \cdot \sigma_0$

σ_{pe}: atomic photoeffect cross section; σ_{coh}: Rayleigh cross section; σ_{incoh}: incoherent scattering cross section.

Chemical element mass attenuation coefficient $\frac{\mu}{\rho}$:

$$\frac{\mu}{\rho} = \frac{\sigma_{total}}{u \cdot A}$$

μ: attenuation factor; ρ:element density; $u = 1.6605402 \times 10^{-24}$g ; A: relative atomic mass of the target element.

Material consisting of compounds:

$$\frac{\mu}{\rho} = \sum_{i=1}^{m} \alpha_i \left(\frac{\mu}{\rho}\right)_i$$

α : fraction by weight of the ith atomic constituent.

Fig. 3: Mathematical derivation for correction steps 1-3.

X-ray intensity after passing through single material object:

$$I_{mono} = I_0 e^{-\int \mu ds} \qquad e^{-\int \mu ds} \Rightarrow f(\mu, d)$$

$$I_{poly} = \int I_0(E) e^{-\int \mu(s,E) ds} dE \qquad \int e^{-\int \mu(s,E) ds} dE \Rightarrow g(\mu, d)$$

X-ray intensity after passing through N-material objects:

$$I_{N,mono} = I_0 \cdot f_1(\mu, d) \cdot f_2(\mu, d) \cdots f_N(\mu, d)$$
$$I_{N,poly} = I_0 \cdot g_1(\mu, d) \cdot g_2(\mu, d) \cdots g_N(\mu, d)$$

Final correction:

$$I_{correction} = \frac{I_{mono}}{I_{poly}} \cdot I_{original}$$

Fig. 4: Mathematical derivation for correction steps 4 and 5.

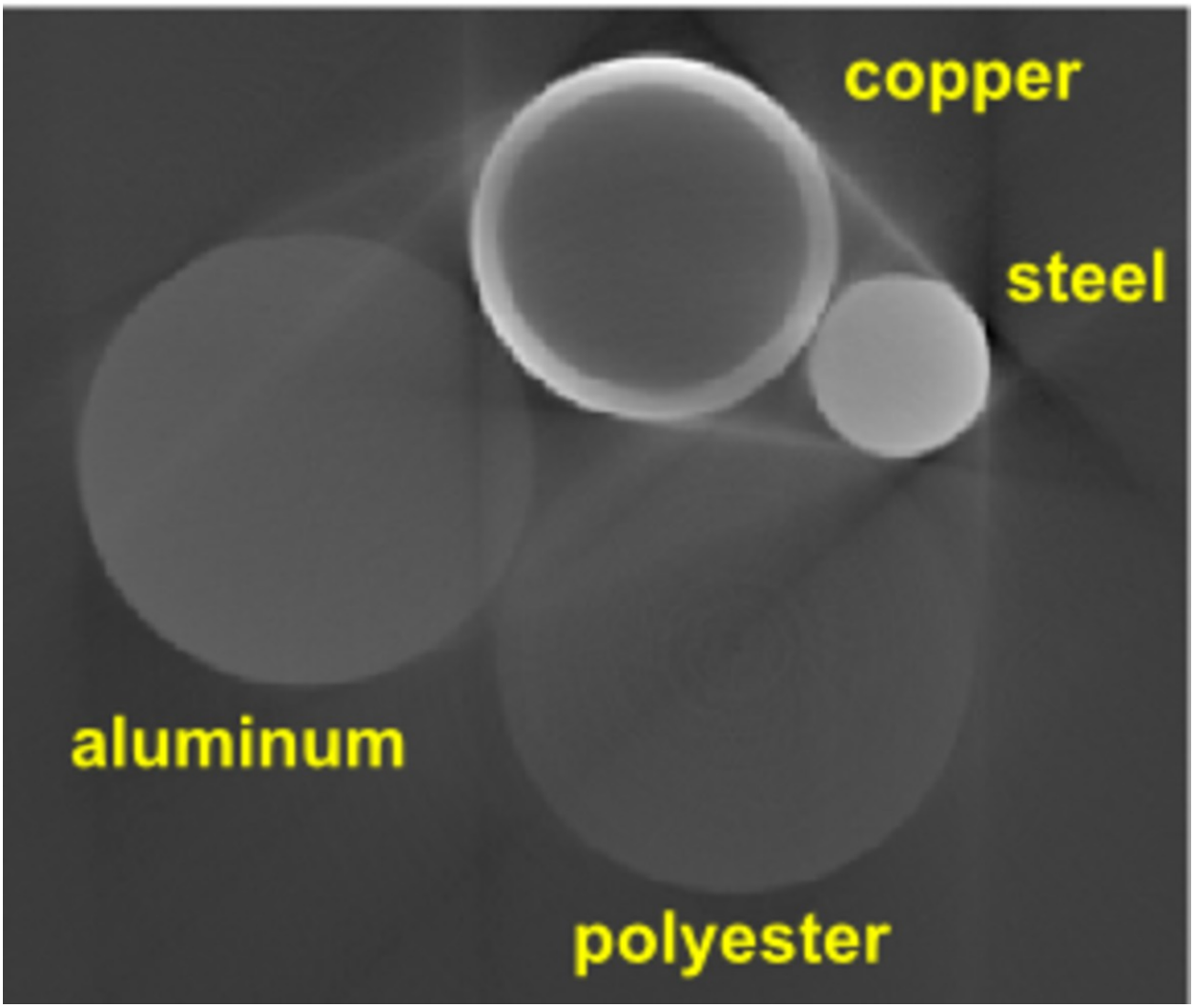

Fig. 5: Reconstruction slice image without BHC. Material placement in volume are indicated.

	Parameters	Value
Trajectory	Source-Detector distance	1400mm
	Source-Object distance	800mm
Source	Tube voltage	120 kV
Detector	Number of pixels	512x512
	Pixel resolution	0.4mm
Volume	Number of voxels	400x400x600
	Voxel size	0.5mm

Table 1: Experimental setup parameters.

Results

Correction results are evaluated focusing cupping and streaking artifacts.

Cupping artifacts:

Fig. 6 on page 9 shows the reconstruction slices after BHC at iteration 1, 4 and 7 (above). Yellow lines are plotted in oder to exam cupping artifacts in copper and steel cylinders, and corresponding line profiles are shown below. It can be observed that cupping artifacts have been significantly removed during iterations. Meanwhile, the differences of object density levels are improved, which can further improve segmentation accuracy for next iteration.

Streaks between objects:

Correction results with focus on streaks between objects are displayed in Fig. 7 on page 10. The fluctuated part at the two sides of steel cylinder are of interest, since the copper cylinder with highest density has largest impact on other objects. After iterative corrections, a significant improvement in terms of reducing streak artifacts can be achieved.

Computational time:

- The processing time for one iteration is less than 30 seconds with detector pixel counts 512x512.
- For each iteration, forward and backward projection modules constitute dominant part for large computational intensity. After efficient GPU-based implementation, forward and backward projections make up about 85% of the total runtime.

Images for this section:

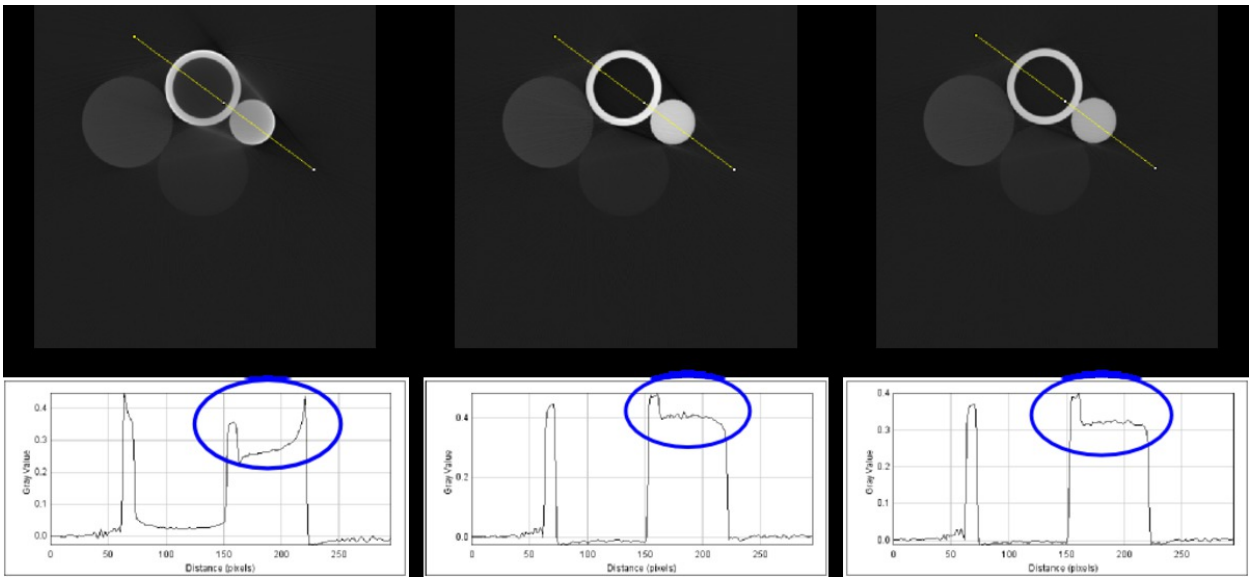

Fig. 6: Correction results focus on cupping artifacts.

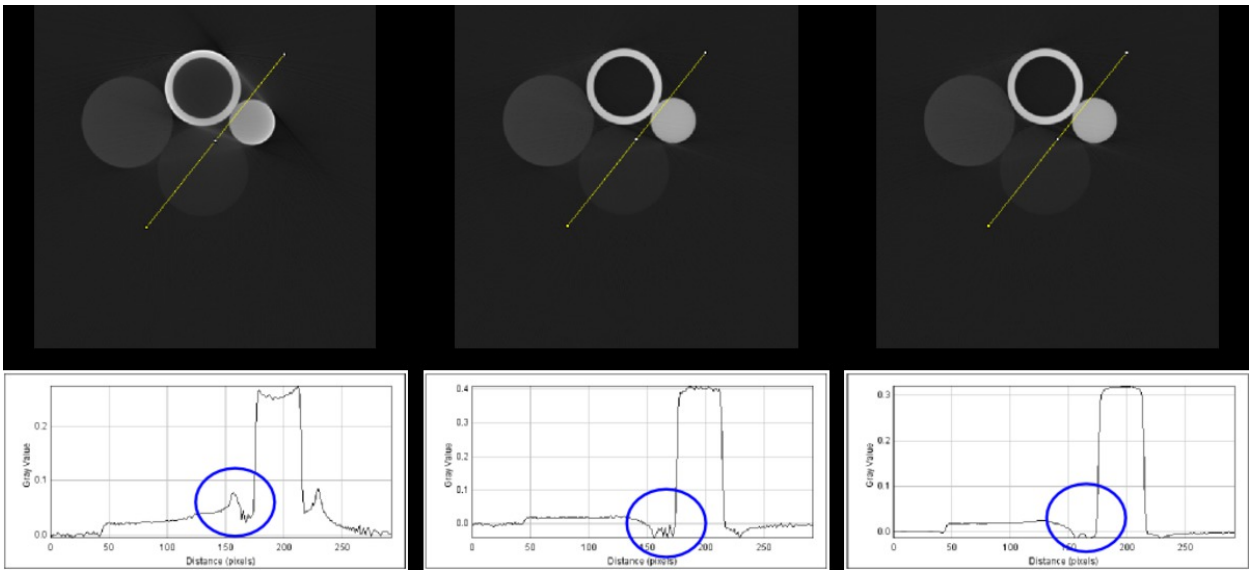

Fig. 7: Correction results focus on streak artifacts.

Conclusion

In this study, we have presented a quantitative cone beam CT beam hardening correction approach which can be applied to datasets consisting of multiple materials.

- The correction results indicated that our approach can significantly improve CT image quality with datasets consisting of multiple materials.
- It has a major contribution of beam hardening artifact suppression when dealing with wide range of object densities, even if segmentation accuracy of preliminary reconstruction image is poor.
- By using an efficient GPU implementation, significant reduction of processing time was achieved. This is a significant practical advantage compared to most other BHC methods, with realization of full cone beam geometry correction for clinical data.

Acknowledgment:

The authors are grateful to Prof.Dr.-ing. Til Aach for his valuable comments.

References

[1] M. Slaney, Principles of Computerized Tomographic Imaging. Society for Industrial Mathematics, 2001.

[2] J. Hsieh, vances.Computed tomography: Principles, design, artifacts, and recent ad- Society of Photo Optical, 2003.

[3] T. M. Buzug, Beam CT. Computed Tomography - From Photon Statistics to Modern Cone-Beam CT. Springer Berlin, 2008.
[4] W. Kalender, "Computed tomography", Erlangen, 2005.
[5] E. V. de Casteele, "Model-based approach for beam hardening correction and resolution measurements in microtomography", Ph.D. dissertation, University Antwerpen, 2004.
[6] F. Kelcz, "Noise considerations in dual energy ct scanning", Medical Physics, vol. vol.6, no.5, pp. 418425, 1979.
[7] N. Menvielle, "Reduction of beam-hardening artifacts in x-ray ct," Engineering in Medicine and Biology Society, Engineering vol. IEEE-EMBS 2005, pp. 18651868, 2005.
[8] M. Krumm, "Reducing non-linear artifacts of multi-material objects in industrial 3d computed tomography," NDT&E International, vol. Vol 41, No 4, pp. pp 242251, 2008.

[9] G. van Gompel, "Towards accurate image reconstruction from truncated x-ray ct projections," Ph.D. dissertation, University Antwerpen, 2009.
[10] E. V. de Casteele, "An energy-based beam hardening model in tomography," Phys.Med.Biol, vol. 47, pp. 41814190, 2002.
[11] M. Krumm, "Referenceless beam hardening correction in 3d computed tomography images of multi-material objects," in 17th World Conference on nondestructive Testing, 25-28.10.2008.
[12] K. V. Slambrouck, "Iterative correction of beam hardening artifacts in ct," 2010.
[13] J. Stonestrom, R. Alvarez, and A. Macovski, "A framework for spectral artifact corrections in X-ray CT, Biomedical Engineering," IEEE Transactions on, no. 2, pp. 128141, 1981.
[14] I. Elbakri and J. Fessler, "Segmentation-free statistical image reconstruction for polyenergetic X-ray computed tomography with experimental validation," Physics in Medicine and Biology, vol. 48, p. 2453, 2003.
[15] N. Menvielle, Y. Goussard, D. Orban, and G. Soulez, "Reduction of beam-hardening artifacts in x-ray CT." Engineering in Medicine and Biology So- ciety, 2005. IEEE-EMBS 2005. 27th Annual International Conference of the. hardening artifacts in X-ray CT, in IEEE, 2005, pp. 18651868.
[16] G. Herman, "Correction for beam hardening in computed tomography," Physics in Medicine and Biology, Physics vol. 24, p. 81, 1979.
[17] H. Gao, L. Zhang, Z. Chen, Y. Xing, and S. Li, " Beam hardening correction for middle-energy industrial computerized tomography," Nuclear Science, IEEET ransactions on vol. 53, no. 5, pp. 27962807, 2006.
[18] X. Mou, S. Tang, and H. Yu, Transactions on, Comparison on beam hardening correction of CT based on HL consistency and normal water phantom experiment," in proceedings of SPIE, Pro- vol. 6318, 2006, p. 63181V.
[19] L. Feldkamp, L. Davis, and J. Kress, Practical cone-beam algorithm, Soc. Am. A, J. Opt. vol. 1, no. 6, pp. 612619, Jun. 1984.
[20] Maki, Birnbaum, Chakraborty, Jacobs, Carvalho, and Herman, Renal cyst pseudoenhancement: beam-hardening eects on ct numbers, in Radiology, 1999, pp. 468472.
[21] A. International, Standard guide for computed tomography (ct) imaging, ASTM International, Tech. Rep., 1997.
[24] N. I. of Standards and Technology, Nist, the national institute of standards and technology.

http://physics.nist.gov/physrefdata/xraymasscoef/cover.html, 2011.

Personal Information

Qiao Yang

Contact: qiao.yang@informatik.uni-erlangen.de